Using Embedded Element Patterns to Improve Aperture Array Calibration

Stefan J. Wijnholds
R&D
ASTRON
Dwingeloo, The Netherlands
wijnholds@astron.nl

Michel Arts
R&D
ASTRON
Dwingeloo, The Netherlands
arts@astron.nl

Pietro Bolli
Arcetri Astrophysical Observatory
INAF
Florence, Italy
pbolli@arcetri.inaf.it

Paola Di Ninni
Arcetri Astrophysical Observatory
INAF
Florence, Italy
dininni@arcetri.inaf.it

Giuseppe Virone
IEIIT
CNR
Turin, Italy
giuseppe.virone@ieiit.cnr.it

***Abstract*—Several existing and planned low-frequency (< 350 MHz) radio astronomical facilities exploit subarrays or *stations* consisting of receiving elements in an irregular configuration. Calibration of the RF path of each receiving element is crucial for accurate beamforming with these stations. Currently used station calibration methods usually assume that the embedded element patterns (EEPs) of the receiving elements within a station are identical. In this contribution, we show that ignoring the inter-element EEP variations causes systematic errors in the calibration results using the stations of the low-frequency receiving systems of the Square Kilometre Array (SKA) and the Low Frequency Array (LOFAR) as examples. We show that the magnitude of these errors increases with increasing EEP variations. We also discuss the challenges faced by SKA and LOFAR to mitigate these errors by exploiting a priori knowledge of the EEPs.**

***Index Terms*—antenna arrays, radio astronomy, mutual coupling, antenna radiation patterns, calibration**

I. Introduction

Several existing and planned low-frequency (<350 MHz) radio astronomical facilities exploit subarrays (often referred to as *stations*) consisting of receiving elements in an irregular configuration. Examples are the Low Frequency Array (LOFAR) [1], the low-frequency instrument of the Square Kilometre Array (SKA-LOW) [2] and the Long Wavelength Array (LWA) [3]. Calibration of the RF path of each receiving element is crucial for accurate beamforming with the (sub)arrays. Currently used calibration methods usually assume that the directional response of the receiving elements is identical [4]–[6]. In practice, this does not hold due to mutual coupling between the receiving elements in an irregular configuration [7]. In this contribution, we show that ignoring the differences between the embedded element patterns (EEPs) of the individual receiving elements leads to systematic errors in the calibration results. We show that the magnitude of these errors increases with increasing EEP variations. We also discuss the challenges faced by SKA and LOFAR to mitigate these errors by exploiting a priori knowledge of the EEPs.

To get a clear view on the issue identified above, we describe the commonly used data model used for station-level calibration in the next section and compare it with a data model that takes EEP variations into account properly. In Sec. III, we assess the impact of ignoring EEP variations for SKA-LOW using numerical data as simulations provide a nice tool to isolate a specific effect. We also provide an analysis for LOFAR in Sec. IV and explain why attempts to improve LOFAR station calibration by using a priori knowledge of the EEPs have hitherto been unsuccessful. We conclude by discussing the implications for station calibration of radio interferometers like LOFAR and SKA that consist of multiple stations.

II. Station calibration

The far-field response of the pth antenna feed can be described by the 2-element vector $\mathbf{E}_p(\mathbf{l})$, whose two elements describe the antenna response in two orthogonal polarisations. The 2-element vector $\mathbf{l}$ represents the direction in two coordinates. If the signal received from direction $\mathbf{l}$ is described by the 2-element vector $\mathbf{s}(\mathbf{l}, t)$, the output voltage of the receive path of the pth feed in the array can be described by

$$v_p(t) = g_p \int \mathbf{E}_p(\mathbf{l}) \cdot \mathbf{s}(\mathbf{l}, t)\, \mathrm{e}^{\mathrm{j}\frac{2\pi}{\lambda}\mathbf{l}\cdot\mathbf{x}_p} \mathrm{d}\mathbf{l}, \tag{1}$$

where $\mathbf{x}_p$ is the position of the pth element, g_p is the overall complex valued gain of the pth receive path (consisting of.amplifiers, cables, analog filters, etc.) and λ is the wavelength of the received signals. In reality, signals are received over a range of frequencies but for brevity of notation, we concentrate on a single, narrowband measurement frequency. This allows us to describe the geometrical delay across the array with a phasor.

Stations usually consist of dual-polarised antennas with parallel feed orientations across the array. As astronomical sources with sufficient signal strength to calibrate individual

antennas within a station are typically unpolarised, station calibration is normally done for each polarisation separately. We can therefore simplify the integrand in (1) by considering the antenna gain to unpolarised radiation $E_p(\mathbf{l}) = \|\mathbf{E}_p(\mathbf{l})\|$ and the source strength $s(\mathbf{l},t) = \|\mathbf{s}(\mathbf{l},t)\|$ such that

$$v_p(t) = g_p \int E_p(\mathbf{l})\, s(\mathbf{l},t)\, \mathrm{e}^{\mathrm{j}\frac{2\pi}{\lambda}\mathbf{l}\cdot\mathbf{x}_p} \mathrm{d}\mathbf{l}. \tag{2}$$

The received signals as described by (2) can be stacked in a vector $\mathbf{v}(t) = [v_1(t), v_2(t), \cdots, v_P(t)]^T$, where P is the number of antennas in the array. These signals are correlated to form the array covariance matrix

$$\mathbf{R} = \mathcal{E}\left\{\mathbf{v}(t)\,\mathbf{v}^H(t)\right\}, \tag{3}$$

where $\mathcal{E}\{\cdot\}$ denotes an expected value.

If the array covariance matrix is evaluated using (2), the directional response of the individual antennas in the array is properly taken into account. In practice, it is often assumed that all EEPs are identical. To describe this assumption, we calculate the average EEP

$$\widetilde{E}(\mathbf{l}) = \frac{1}{P}\sum_{p=1}^{P} E_p(\mathbf{l}) \tag{4}$$

and use it to describe the calibration model of the received signals as

$$\widetilde{v}_p(t) = g_p \int \widetilde{E}(\mathbf{l})\, s(\mathbf{l},t)\, \mathrm{e}^{\mathrm{j}\frac{2\pi}{\lambda}\mathbf{l}\cdot\mathbf{x}_p} \mathrm{d}\mathbf{l}. \tag{5}$$

The calibration model for the array covariance matrix based on (5) is

$$\widetilde{\mathbf{R}}(\mathbf{g}) = \mathcal{E}\left\{\widetilde{\mathbf{v}}(t)\,\widetilde{\mathbf{v}}^H(t)\right\}, \tag{6}$$

where $\mathbf{g} = [g_1, g_2, \cdots, g_P]$ is the vector of gains to be estimated by calibration. That estimation problem can be formulated as

$$\widehat{\mathbf{g}} = \underset{\mathbf{g}}{\operatorname{argmin}} \left\|\mathbf{R} - \widetilde{\mathbf{R}}(\mathbf{g})\right\|, \tag{7}$$

where we re-emphasise that $\mathbf{R}$ is calculated based on (2) and $\widetilde{\mathbf{R}}$ based on (5). If the source structure described by $s(\mathbf{l},t)$ is known, fast algorithms are available to solve this quadratic problem [4].

III. Impact analysis for SKA-LOW

Variations between the EEPs of the antennas within an array are expected to increase when the array becomes more compact as that will increase the strength of electro-magnetic (EM) coupling between the antennas. The impact of EEP variations is therefore expected to be larger in more compact arrays. Unfortunately, compact arrays also have a low spatial resolution and are therefore very sensitive to sky background temperature variations on large angular scales, which include, in particular, the diffuse structure of our own Galaxy. As the sky background temperature is hard to model, it is difficult to disentangle the effects of sky background temperature modelling errors from the effects of EEP modelling errors when experimenting with actual data from, e.g., a LOFAR station. This is discussed in more detail in Sec. IV. We therefore decided to use simulations for our assessment of the impact of EEP variations on station calibration accuracy.

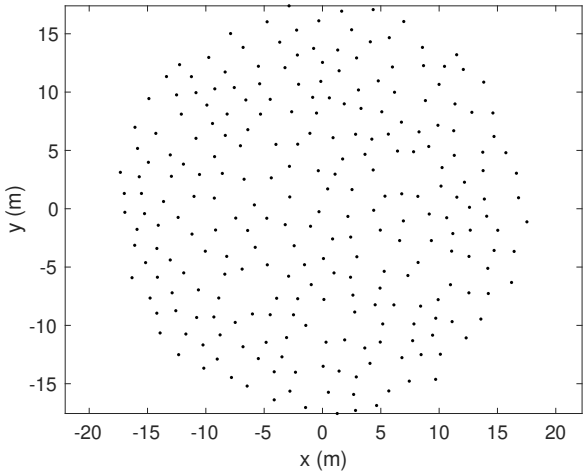

Fig. 1. SKA-LOW station array layout with 256 antennas.

In our simulations, we consider calibration of a single SKA-LOW station on the SKA-site in Australia consisting of 256 SKALA4AL antennas, one of the log-periodic antenna designs proposed for SKA-LOW [8]. The array configuration is shown in Fig. 1. To show the impact of reduced EEP variations, we will also show results for an array of bowtie antennas in the same configuration that exhibit smaller EEP variations [9]. It should be noted that the length of the lower dipole of the SKALA4AL antenna is about 1.6 m, whereas the considered bowtie length is about 0.7 m. Therefore, we are comparing two solutions with different sensitivity levels and bandwidths. Nevertheless, this comparison is relevant for the sake of the analysis presented hereafter. Figure 2 shows the RMS deviation between the 256 EEPs across the sky relative to the peak gain of the average EEP for both cases at 110 MHz, clearly showing that the inter-element EEP differences are about an order of magnitude less for the array of bowtie antennas as compared to the array of SKALA4AL antennas. The frequency of 110 MHz was chosen as both EM simulations were done (a.o.) at that frequency, so interpolation across frequency was not needed in either case. Also, the calibration requirements for SKA-LOW are most stringent around that frequency [10].

We used the map from the 408-MHz Haslam survey [11] to obtain a realistic source model, including the spatial variations of the sky background noise temperature. This temperature map was converted to a map of discrete sources representing the total flux in each pixel to evaluate the integral over the source structure in the sky weighted by the EEP for each element in (2). The fluxes were scaled from 408 MHz to the simulation frequency of 110 MHz by applying a correction based on the average sky background temperature spectrum. The flux in each pixel was treated as an independent source signal, i.e., the signal from each pixel was assumed to be

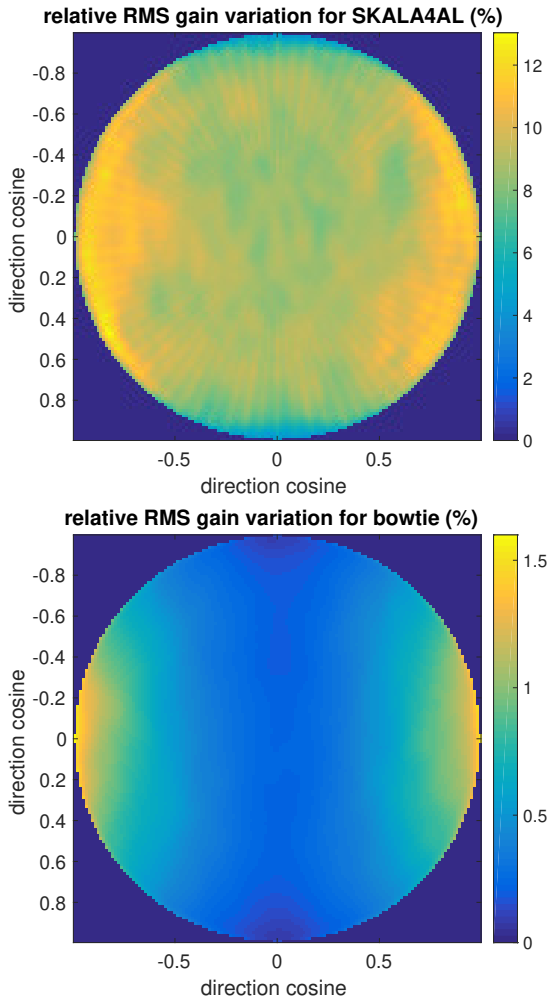

Fig. 2. RMS EEP gain variations across the entire visible sky expressed as percentage of the peak gain of the average EEP for a SKA-LOW station consisting of SKALA4AL antennas (top) or bowtie antennas (bottom).

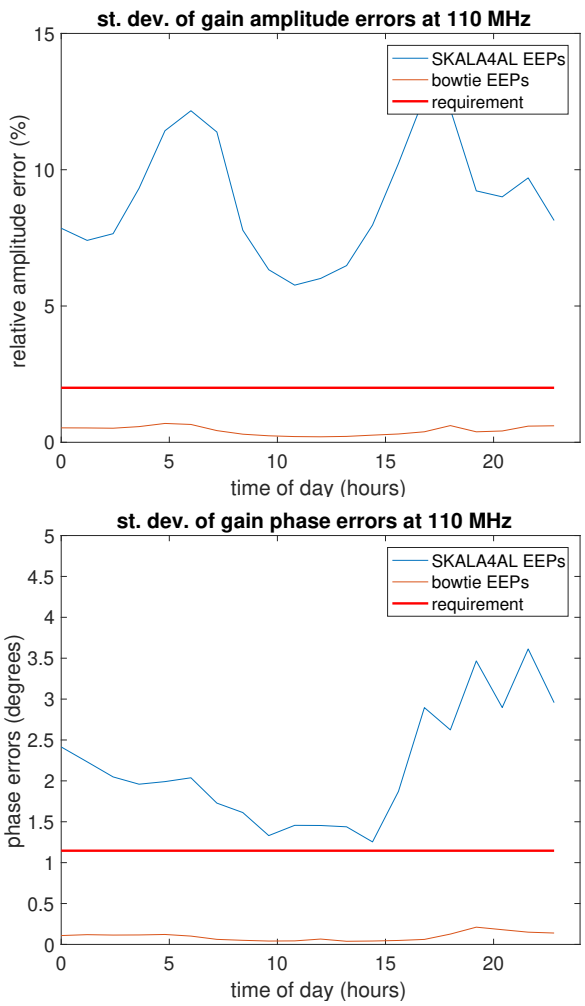

Fig. 3. RMS gain amplitude (top) and phase (bottom) estimation error across the array during a single day. The red line indicates the calibration accuracy requirement derived for the SKA-LOW stations [10].

uncorrelated. The array covariance matrix calculated based on this model, $\mathbf{R}$, was considered as "measured" array covariance matrix.

This procedure was repeated while assuming that all EEPs were identical to the average EEP as described by (5). The resulting array covariance matrix, $\widetilde{\mathbf{R}}$, was considered as the "model" array covariance matrix. The impact of ignoring the variations between the EEPs can now be determined by estimating "gains" from the difference between the measured and model array covariance matrix as described by (7). As the dominant sources in the sky move w.r.t. the array during a day and the EEP variations are not equally severe in all directions as shown by Fig. 2, we expect the gain errors to vary with time of day. The simulation was therefore repeated for 20 instances in time over a 24-hour period.

Figure 3 shows the simulation results in terms of the RMS gain amplitude and phase errors across the 256-elements in the array. Based on these simulation results, over a full day, the calibration errors caused by ignoring the differences between the EEPs of the individual antennas are typically a factor 23 lower for the amplitude estimates and a factor 26 lower for the phase estimates for the array of bowtie antennas as compared to the array of SKALA4AL antennas. This seems quite consistent with the factor 25 lower RMS variability across the sky between the EEPs of the bowtie antennas compared to the EEPs of the SKALA4AL antennas as shown in Fig. 2. This indicates that the systematic errors produced by ignoring the differences between the EEPs scale with the magnitude of the inter-element EEP variations, as expected. The curves show a significant variation with time. This can be explained by the rise and set of the Galactic plane. If the dominant amount of flux is received from the directions where the EEPs have the largest variability (see Fig. 2), the gain calibration errors reach a peak.

The assumption that the directional response is the same for all the antennas in the array obviously simplifies the construction of a suitable model for the calibration data as illustrated by the difference betwen (5) and (2). We note that

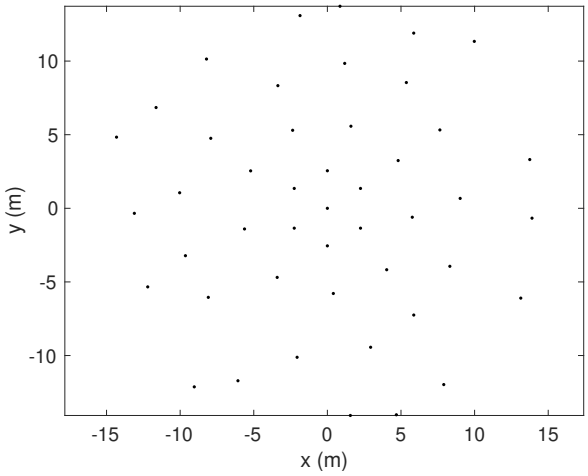

Fig. 4. Compact LOFAR LBA station array layout with 46 antennas.

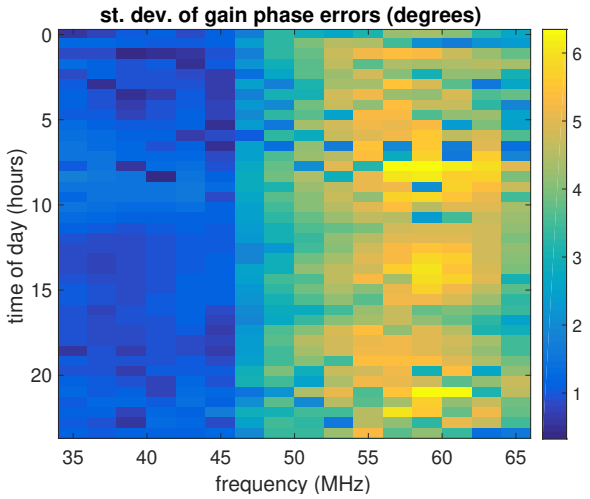

Fig. 5. Standard deviation of the phase errors on the elements of the array due to ignoring EEP variations between those elements as a function of time of day and frequency.

(2) is already a simplification of the polarised description given by (1) that removes any phase variation among the EEPs. Although this is a second order effect, it implies that Fig. 3 likely underestimates the errors by a small amount. As the results shown in Fig. 3 indicate that the magnitude of the systematic errors caused by this assumption decreases with decreasing inter-element EEP variations, an obvious strategy to mitigate these systematic errors is to reduce inter-element EEP variations by design. In our example, opting for an array of bowtie antennas instead of log-periodic antennas would reduce them by roughly a factor 25. Unfortunately, this is not always feasible due to other requirements that also need to be satisfied such as sensitivity and bandwidth. In that case, a properly validated EM model of the antenna array is required that can be used to calculate the EEPs of the individual antennas needed to evaluate (2). Validation of an EM model is a significant amount of work [7]. That model then needs to be used to describe the EEPs in sufficient detail to allow quick evaluation for a specific direction and frequency during the calibration process. This all requires considerable computing resources. Abandoning the assumption that all EEPs are identical thus incurs significant costs.

IV. Impact analysis for LOFAR

LOFAR is an important pathfinder for SKA-LOW as it covers a similar frequency range and has a similar system architecture. It is particularly interesting to note that the Dutch LOFAR stations have an observing mode that exploits a compact 35-m diameter configuration of Low Band Antennas (LBA) consisting of 46 antennas to observe in the 30 – 90 MHz range. This configuration, shown in Fig. 4, is almost identical in size to the envisaged SKA-LOW stations and follows a similar station layout concept (randomised configuration), albeit with fewer antennas. In view of the similarities, LOFAR is an important testbed to demonstrate the proposed calibration procedures for SKA-LOW. In the context of the issue discussed in this paper, it would be interesting to demonstrate improved LBA station calibration by taking into account the differences between the EEPs.

To assess the impact of EEP variations on LOFAR station calibration, the simulation described above was repeated for the LOFAR case using an EM model for the LBA station that was validated by drone measurements as described in [7]. The EM model provided predicted EEPs at the drone-measurement frequencies of 31.8, 44.5, 57.2 and 69.9 MHz. The simulations were done over the interval from 35 MHz to 65 MHz in steps of 2 MHz using linear interpolation between the drone-measurement frequencies. The expected phase error made across the elements of the array by ignoring the EEP variations between the elements is shown in Fig. 5. The results indicate that the errors are largest near 57 MHz (about 5 degrees). This was expected as this is the resonance frequency of the antennas, where the inter-element coupling and, hence, the variations between the EEPs are largest [12]. This is illustrated by the RMS EEP gain variations at 40 and 57 MHz as predicted by the EM model by linear interpolation across frequency as shown in Fig. 6.

In simulations, we can calculate the statistics of the calibration error over the elements of the array by treating the error on each element as one realisation of the error distribution. In a practical experiment, we cannot calculate the error on individual elements as we do not know the ground truth. We can, however, assume that the instrument is temporally stable and treat consecutive measurements in time as realisations of the underlying error distribution. In the case of LOFAR, the cables between the antennas and the receiver units are buried into the ground and the receiver units are placed in a temperature-controlled enclosure. This ensures a very stable receive path response with gain variations of at most 1% to 1.5% over a day. Figure 7 therefore shows the expected phase errors per receive path as function of frequency caused by ignoring the EEP variations, where the standard deviation was

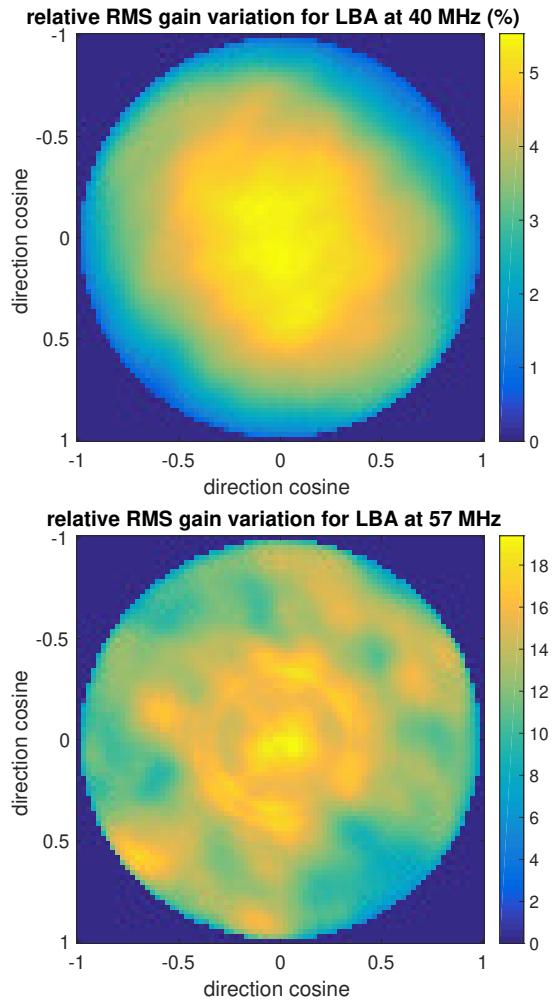

Fig. 6. RMS EEP gain variations across the entire visible sky expressed as percentage of the peak gain of the average EEP for the LBAs in the compact configuration at 40 MHz (top) and 57 MHz (bottom).

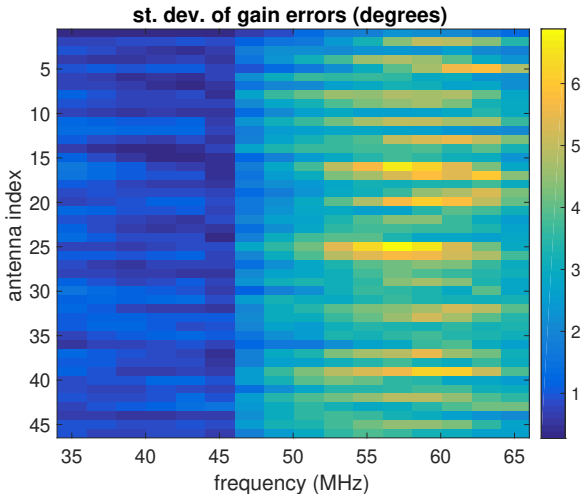

Fig. 7. Standard deviation of the phase errors of the individual receive paths due to ignoring EEP variations between the receiving elements as a function of frequency. The standard deviation was calculated by treating each instance in time as a realisation of the underlying error distribution.

calculated over the 40 time instances spanning 24 hours. The results indicate that, below 45 MHz, the expected RMS errors are as small as $\sim 1^\circ$ and that around the resonance peak, the errors rise to $\sim 5^\circ$.

So far, attempts to improve LOFAR LBA station calibration by taking the EEP variations into acount, thereby removing the error depicted in Figs. 5 and 7, have been inconclusive. This is likely due to inaccuracies in the source model used. To start with, the diffuse emission was modeled based on the 408-MHz Haslam survey [11] assuming that the spectral behaviour of the diffuse emission is the same across the sky, such that the flux ratio between different regions does not change with frequency. There is some observational evidence that this does not hold [13]. Moreover, compact sources like Cassiopeia A and Cygnus A, may suffer from ionospheric scintillation causing the apparent flux to change with time [14]. The impact of ionospheric propagation conditions aggravates towards the lowest frequencies and these conditions are therefore particularly important for measurements below 100 MHz [15], [16]. In view of the outcome of our experiment, it is likely that, in the LOFAR case, source modelling errors are equally significant as instrument modelling errors and that further improvements to the source model used for calibration is needed first to improve LOFAR LBA station calibration.

V. Conclusions

Many low-frequency (< 350 MHz) radio astronomical facilities consist of (sub)arrays of antenna elements placed in an irregular configuration. Most currently used calibration methods assume that the EEPs of the antennas can be considered identical. In this paper, we assessed the impact of this assumption for the stations of SKA-LOW and LOFAR and found that this assumption may cause significant systematic errors in the calibration results, in particular when using antenna types for which there is significant EM coupling between the antennas over at least a portion of the operational frequency range. However, our attempt to demonstrate improvement by including a priori knowledge of the EEPs calculated by a validated EM model in LOFAR station calibration was unsuccessful. This was explained by inaccuracies in the source models currently available for compact arrays and ionospheric propagation conditions. This shows that calibration of SKA-LOW will require a significant effort to obtain an accurate source model and an accurate EM model for the instrument. It may be possible to relax the source model requirements by calibrating receiving elements distributed over multiple stations simultaneously. However, this will still require a validated EM model for the EEPs of the individual elements, which is already a formidable task in itself.

VI. Acknowledgement

The authors would like to thank Daniel Ung for providing the EEPs for a SKA-LOW station of bowtie antennas.

This work was supported in part by the National Institute for Astrophysics under Program TECNO INAF 2014 and in part by the Netherlands Organization for Scientific Research.

REFERENCES

[1] M. P. van Haarlem *et al.*, "LOFAR: The Low Frequency Array," *Astronomy & Astrophysics*, vol. 556, no. A2, pp. 1–53, Aug. 2013.

[2] P. E. Dewdney, P. J. Hall, R. T. Schilizzi, and T. J. L. W. Lazio, "The Square Kilometre Array," *Proceedings of the IEEE*, vol. 97, no. 8, pp. 1482–1496, Aug. 2009.

[3] S. W. Ellingson *et al.*, "The Long Wavelength Array," *Proceedings of the IEEE*, vol. 97, no. 8, pp. 1421–1430, Aug. 2009.

[4] S. Salvini and S. J. Wijnholds, "Fast gain calibration in radio astronomy using alternating direction implicit methods: Analysis and applications," *Astronomy & Astrophysics*, vol. 571, no. A97, pp. 1–14, Nov. 2014.

[5] A. P. Beardsley, N. Thyagarajan, J. D. Bowman, and M. F. Morales, "An efficient feedback calibration algorithm for direct imaging radio telescopes," *Monthly Notices of the Royal Astronomical Society*, vol. 470, no. 4, pp. 4720–4731, Oct. 2017.

[6] S. Chiarucci and S. J. Wijnholds, "Blind calibration of radio interferometric arrays using sparsity constraints and its implications for self-calibration," *Monthly Notices of the Royal Astronomical Society*, vol. 474, no. 1, pp. 1028–1040, Feb. 2018.

[7] G. Virone *et al.*, "Strong Mutual Coupling Effects on LOFAR," *IEEE Transactions on Antennas and Propagation*, vol. 66, no. 5, pp. 2581–2588, May 2018.

[8] P. Di Ninni, M. Bercigli, P. Bolli, G. Virone, and S. J. Wijnholds, "Mutual Coupling Analysis for a SKA1-LOW Station," in *13th European Conference on Antennas and Propagation*, Krakow, Poland, 31 Mar. – 5 Apr. 2019.

[9] D. Ung, "Embedded Element Pattern Beam Model for the Murchison Widefield Array," International Centre for Radio Astronomy Research (ICRAR), Perth, Australia, Tech. Rep., 16 Sep. 2016.

[10] S. J. Wijnholds, "L1 and L2 Stability Requirements for SKA-LOW," SKA Office, Manchester, UK, Tech. Rep. SKA-TEL-LFAA-0200011, 9 Jun. 2016.

[11] C. Haslam, C. Salter, H. Stoffel, and W. Wilson, "A 408 MHz all-sky continuum survey II - The atlas of contour maps," *Astronomy & Astrophysics Supplement Series*, vol. 47, pp. 1–2, 4–51, 53–142, Jan. 1982.

[12] P. Di Ninni, P. Bolli, F. Paonessa, G. Pupillo, G. Virone, and S. J. Wijnholds, "Electromagnetic Analysis and Experimental Validation of the LOFAR Radiation Patterns," *International Journal of Antennas and Propagation*, vol. 2019, no. 9191580, pp. 1–12, Jan. 2019.

[13] K. Maeda, H. Alvarez, J. Aparici, J. May, and P. Reich, "A 45-MHz continuum survey of the northern hemisphere," *Astronomy & Astrophysics Supplement Series*, vol. 140, no. 2, pp. 145–154, Dec. 1999.

[14] P. Prasad, S. J. Wijnholds, F. Huizinga, and R. A. M. J. Wijers, "Real-time calibration of the AARTFAAC array for transient detection," *Astronomy & Astrophysics*, vol. 568, no. A48, pp. 1–18, Aug. 2014.

[15] S. T. Loi *et al.*, "Power spectrum analysis of ionospheric fluctuations with the Murchison Widefield Array," *Radio Science*, vol. 50, no. 7, pp. 574–597, Jul. 2015.

[16] M. Mevius *et al.*, "Probing ionospheric structures using the LOFAR radio telescope," *Radio Science*, vol. 51, no. 7, pp. 927–941, Jul. 2016.